Electronic structure of $EuPd_2Si_2$ in the vicinity of the critical endpoint

O. Fedchenko,[1,5] Y.-J. Song,[2] O. Tkach,[1] Y. Lytvynenko,[1,3] S. V. Chernov,[4] A. Gloskovskii,[4] C. Schlueter,[4] M. Peters,[5] Robert Möller,[5] Alexej Kraiker,[5] K. Kliemt,[5] C. Krellner,[5] R. Valentí,[2] G. Schönhense,[1] and H. J. Elmers[1,*]

[1]*Institut für Physik, Johannes Gutenberg-Universität, Staudingerweg 7, D-55128 Mainz, Germany*
[2]*Institut für Theoretische Physik, Goethe-Universität Frankfurt, Max-von-Laue Strasse 1, 60438 Frankfurt am Main, Germany*
[3]*Institute of Magnetism of the NAS and MES of Ukraine, 03142 Kyiv, Ukraine*
[4]*Deutsches Elektronen-Synchrotron DESY, 22607 Hamburg, Germany*
[5]*Physikalisches Institut, Goethe Universität Frankfurt, Max-von-Laue-Strasse 1, 60438 Frankfurt am Main, Germany*

(Received 3 February 2025; revised 17 April 2025; accepted 9 May 2025; published 22 May 2025)

Hard x-ray angle-resolved photoemission spectroscopy reveals significant changes in the valence band states of $EuPd_2Si_2$ at a temperature T_V, where the Eu ions undergo a temperature-induced valence crossover from a magnetic Eu^{2+} state to a low-temperature valence-fluctuating state. The substitution of Pd by Au and Si by Ge results in a decrease in T_V and the emergence of an antiferromagnetic state at low temperatures without valence fluctuations. It has been proposed that the boundary between the antiferromagnetic order and the valence transition represents a first-order phase transition associated with a specific type of second-order critical endpoint. In this scenario, strong coupling effects between fluctuating charge, spin, and lattice degrees of freedom are to be expected. In the case of $EuPd_2(Si_{1-x}Ge_x)_2$ with $x = 0.13$, which is close to the critical endpoint, a splitting of conduction band states and the emergence of flat bands with a restriction along the Γ-X directions have been observed. A comparison with *ab initio* theory shows a high degree of agreement with the experimental results.

DOI: 10.1103/PhysRevB.111.195149

I. INTRODUCTION

The interplay between electronic and structural degrees of freedom in materials with correlated electrons gives rise to interesting phase transitions as evidenced by Gati *et al.* [1]. The study of these unconventional phase transitions allows for not only the exploration of fundamental aspects of solid-state physics, but also the identification of potential technological applications. In the vicinity of a second-order critical end point (CEP), which terminates a first-order phase transition line, strong fluctuations are anticipated [1]. It is of significant interest to tune a material to a CEP, which can be achieved through the application of mechanical pressure or, alternatively, through the introduction of chemical pressure, namely by partial substitution of atoms with isoelectronic atoms of a different size. In this case, strong-coupling effects between the correlated electrons and the lattice degrees of freedom can be expected, resulting in unconventional phenomena such as critical elasticity [1].

The $EuPd_2Si_2$ system has been utilized as a model for investigating valence transitions induced by temperature or pressure [2–6]. Similar valence transitions have been observed in the related compounds $EuCu_2Si_2$ [7,8], and $EuIr_2Si_2$ [9–11] under ambient pressure. At elevated pressures, valence transitions have been observed in $EuRh_2Si_2$ [12], $EuNi_2Ge_2$ [13], and $EuCo_2Ge_2$ [14]. Additionally, partial substitutions of atoms within the crystal lattice may elicit a response analogous to that of pressure [15–18].

In their seminal work, Segre *et al.* [3] presented the first comprehensive phase diagram for $EuPd_2Si_2$ that encompassed both magnetic and valence transitions of this compound. They postulated that the phase diagram could serve as a blueprint for understanding the crossover between the highly magnetic divalent Eu^{2+} state at high temperature and the nonmagnetic trivalent Eu^{3+} state at low temperature. It is currently unclear whether the microscopic driving mechanism for the strong intersite interactions responsible for the cooperative valence transition is predominantly electronic or elastic in nature. This is due to the fact that the broken symmetry at the surface presents an obstacle to surface-sensitive photoemission spectroscopy [19–21].

Upon cooling through the transition temperature of approximately 160 K, a pronounced and continuous valence change from $Eu^{2.8+}$ to $Eu^{2.3+}$ is observed [21–23]. The inflection point of the valence change $V(T)$, designated as T_V, serves as a measure of the energy scale associated with the valence change. $EuPd_2Si_2$ is situated on the high-pressure side of the second-order critical endpoint, as evidenced by magnetic [3] and thermodynamic measurements [18]. The valence transition in $EuPd_2Si_2$ can be tuned by external stimuli, including magnetic fields, pressure, and biaxial strain [24–27]. The availability of single crystals of pristine $EuPd_2Si_2$ [17] and Ge-substituted $EuPd_2(Si_{1-x}Ge_x)_2$ [17,18] has facilitated detailed investigation of the valence transition near the critical endpoint [28].

*Contact author: elmers@uni-mainz.de

The present study examines the electronic band dispersion in the series $EuPd_2(Si_{1-x}Ge_x)_2$ [18], where the replacement of Si by the isoelectric but larger Ge atom corresponds to $EuPd_2Si_2$ at a negative chemical pressure. In this case, the critical regime can be accessed via the doping concentration. For comparison, the series $Eu(Pd_{1-x}Au_x)_2Si_2$ is studied, where the substitution of Pd by the larger and nonisoelectric Au atom also leads to a reduction of T_V.

In this study, hard x-ray angle-resolved photoemission spectroscopy was employed to measure the bulk band structure of $EuPd_2Si_2$ at negative pressure, approaching the critical endpoint of the valence transition. The observation of a flat band accompanied by a splitting of the conduction band indicates the onset of antiferromagnetic order, which is in agreement with the results of density functional calculations.

II. EXPERIMENTAL

Single crystals of the compounds $EuPd_2(Si_{1-x}Ge_x)_2$ and $Eu(Pd_{1-x}Au_x)_2Si_2$, where x denotes the concentration as determined by energy dispersive x-ray spectroscopy (EDX), were synthesized using the Czochralski method from an Eu-rich levitating melt, as previously described in Refs. [17,18]. EDX has been determined at different positions on the sample. We have chosen a small cut (section) of a larger piece with sufficiently constant and homogeneous area. To facilitate the pre-orientation of the crystals, Laue diffractograms were employed as the primary characterization tool. In Frankfurt, the crystals were cut using a spark erosion device using a wire cutter. The single crystals were affixed to the sample holder via epoxy resin, with the (001) plane oriented parallel to the sample holder plate. A stainless steel pin affixed to the surface was utilized for the cleavage process following the introduction of the sample into the ultrahigh vacuum environment. The cleavage was conducted at room temperature under ultrahigh vacuum conditions $<3 \times 10^{-10}$ mbar. The samples were then transferred under vacuum into a He-cooled (25 K) sample stage on a high-precision 6-axis hexapod manipulator of the time-of-flight momentum microscope.

The photoemission experiments were conducted at beamline P22 of the storage ring PETRA III at DESY in Hamburg, Germany [29,30]. The footprint of the photon source is approximately 20×50 μm^2. In the 3 keV range, a Si(220) double-crystal monochromator was employed, yielding a total energy resolution of 100 meV. In the 5 keV range, a Si(331) crystal yielded an energy resolution of 150 meV. The crystals were cleaved in ultrahigh vacuum prior to the photoemission experiments.

One of the most significant advantages of angle-resolved photoelectron spectroscopy in the hard x-ray range is the notable enhancement in the inelastic mean free path of the escaping photoelectrons. Accordingly, the present results represent true bulk properties, which is crucial given that the valency of Eu at the surface of valence fluctuating systems is always divalent, thereby precluding the possibility of studying the valence crossover [9,20,21]. Note, that the measured spectra still include signals from the surface regions with mostly divalent Eu atoms at low temperature. We expect a surface-related contribution of about 10% to the measured spectrum.

To address the limitations of low cross-section and low signal-to-background ratio in the hard x-ray regime, we employed time-of-flight momentum microscopy [31], a technique that enables the highly efficient acquisition of three-dimensional data sets of the photoelectron intensity $I(E_B, k_x, k_y)$ as a function of binding energy, $E_B = -(E - E_F)$, and momentum k_x, k_y. The processing of data to reduce noise limits the resolution of the momentum measurement to 0.08 Å^{-1} for the results presented below.

Photoemission data were acquired for eight hours in each case. The details of the data evaluation procedure are described in Refs. [30,32]. The evaluation and presentation of the band structure data are consistent with those described in Ref. [28].

III. EXPERIMENTAL RESULTS FOR $EuPd_2(Si_{1-x}Ge_x)_2$

The valence number V of the Eu ions is determined at temperatures above and below the valence transition using hard x-ray photoelectron spectroscopy (HAXPES). This is conducted at the Eu 3d core levels at a photon energy of 3.4 keV. The high kinetic energy of photoemitted electrons ensures bulk sensitivity [33]. Figure 1 compares the experimental results for $EuPd_2(Si_{1-x}Ge_x)_2$ with $x = 0$, 0.05, and 0.13. The spin-orbit interaction results in the splitting of the Eu 3d spectrum into two components, an Eu $3d_{5/2}$ and an Eu$3d_{3/2}$, component with a splitting energy of 30 eV. Here, we only present the results for the Eu $3d_{5/2}$ component. The Eu $3d_{5/2}$ component is further split by a chemical shift depending on the valence state, which is either Eu^{2+} or Eu^{3+} with a splitting of 10 eV. The splitting enables the determination of the mean valence from the corresponding peak areas [34].

A notable shift in the ratio between the Eu^{2+} and the Eu^{3+} components is observed for the cases of $x = 0$ and 0.05, indicative of a valence transition. For $x = 0$, an evaluation of the peak area ratio yields valence number values of $V = 2.5$ at low temperature and $V = 2.1$ at high temperature. In the case of partial substitution of Si by Ge with $x = 0.05$, the high-temperature valence number exhibited a minimal change with a value of $V = 2.12$. However, at low temperature, the value increased to $V = 2.74$, indicating an even more pronounced valence transition compared to the pristine sample. For higher Ge concentration of $x = 0.13$, the valence numbers for high and low temperature are nearly identical, at $V = 2.08$ and 2.09, respectively. In this case, the valence transition is not observed.

Figure 2 illustrates the temperature dependence of the valence number for the case of $x = 0.05$, as determined from the HAXPES spectra. The inclination point indicates the valence transition temperature, which is determined to be 100 K. This value is in agreement with the inclination point of the susceptibility curve. However, it should be noted that minor discrepancies may be attributed to the differing experimental setups employed. The transition is not abrupt, but rather occurs within a temperature range between 90 K and 110 K.

The valence band photoemission intensity measurements, as illustrated in Fig. 3, demonstrate the density of states at

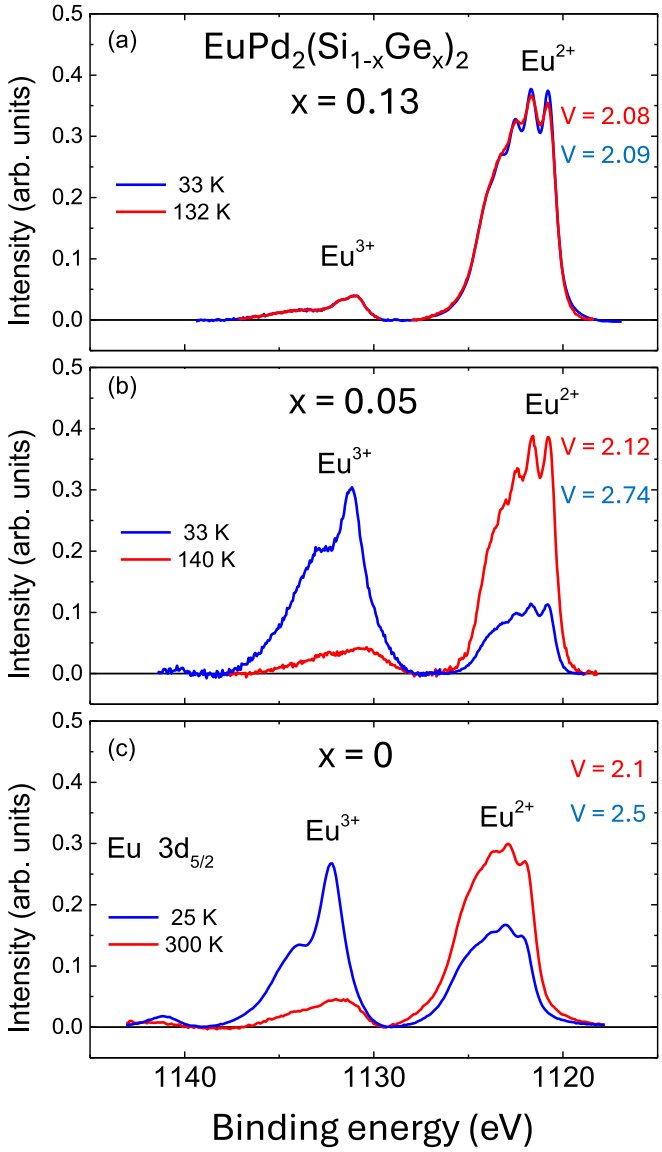

FIG. 1. (a)–(c) Temperature dependence of the Eu $3d_{5/2}$ core level spectra obtained with a photon energy of 3.4 keV at the indicated temperatures for $EuPd_2(Si_{1-x}Ge_x)_2$ single crystals with (c) $x = 0$, (b) 0.05, and (a) 0.13. The Eu valence V is calculated from the ratio of the areas of the corresponding $3d$ core level peaks. The specified binding energies are referred to the Fermi level. Data for $x = 0$ are taken from Ref. [28].

both low and high temperatures. For the sake of comparison, the spectra have been normalized to the maximum at 3.5 eV binding energy. The sharp peak situated in close proximity of the Fermi level can be attributed to the partially filled Eu^{2+} $4f$ states. The observed increase in this peak for $x = 0$ and 0.05 in the high temperature phase is indicative of an increase in the Eu^{2+}/Eu^{3+} ratio. The Eu^{3+} $4f$ multiplet states are responsible for the two minor peaks observed between 6 and 8 eV binding energy at low temperature, which are no longer present at high temperature [20,35]. The valence spectra also corroborate the existence of an almost pure magnetic Eu^{2+} state for temperatures exceeding the valence transition temperature ($T > T_V$) and a pronounced redistribution of the peak heights upon

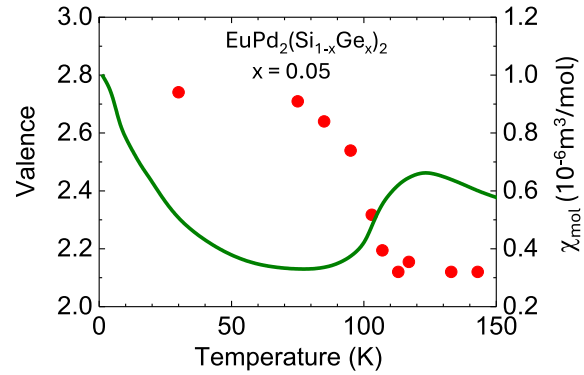

FIG. 2. Temperature dependence of Eu valence for $EuPd_2(Si_{1-x}Ge_x)_2$ with $x = 0.05$ as determined from the Eu HAXPES spectra (red points, left scale). Molar susceptibility as a function of temperature, indicating a similar transition temperature (green curve, right scale).

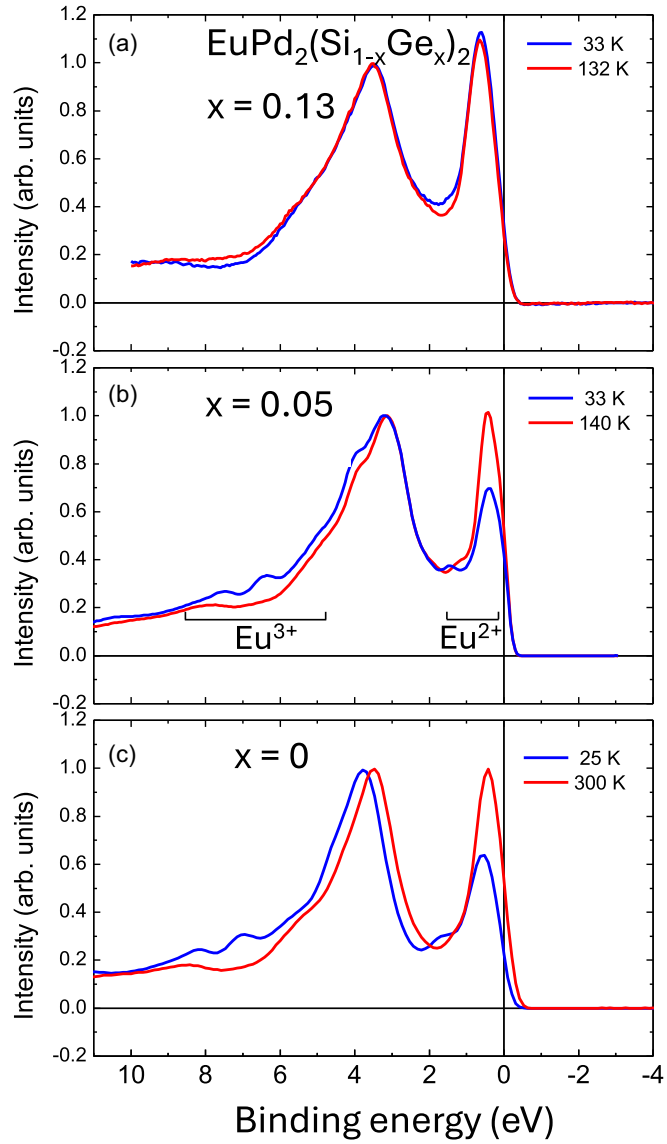

FIG. 3. Valence band energy distribution curves for the indicated temperatures and samples. The photoemission intensity was integrated over a planar section of the full Brillouin zone.

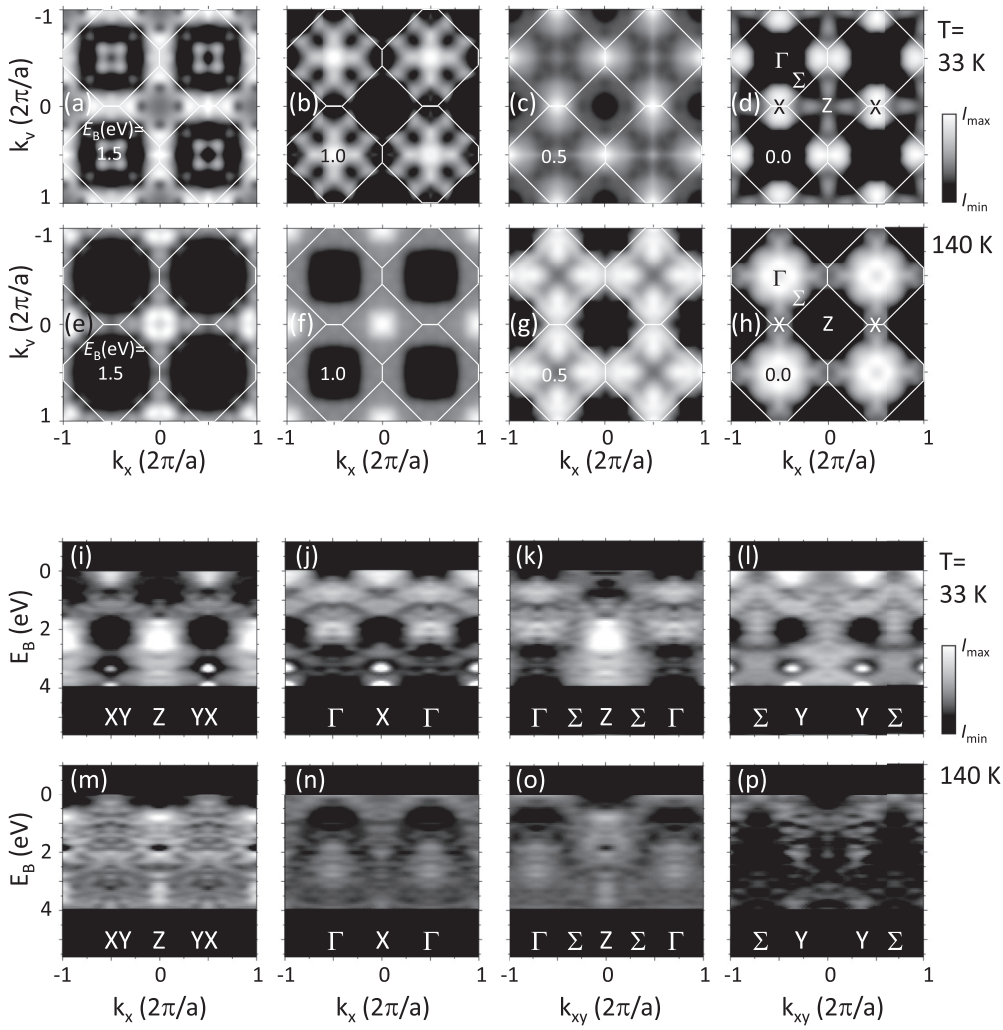

FIG. 4. (a)–(h) $EuPd_2(Si_{1-x}Ge_x)_2$ with $x = 0.05$. Constant energy maps of the photoemission intensity $I(E_B, k_x, k_y)$ for the indicated binding energies E_B measured at 33 K (a)–(d) and 140 K (e)–(h). The photon energy is 3.4 keV. The photoemission intensity has been symmetrized according to the crystal symmetry. (i)–(p) Binding energy versus parallel momentum sections of the photoemission data array along the indicated high symmetry directions measured at 33 K (i)–(l) and 140 K (m)–(p). The photoemission intensity is normalized on the valence band energy distribution curve shown in Fig. 3(b) and color coded on the indicated linear black-white scale.

cooling below T_V. These findings align with the observations made on polycrystalline $EuPd_2Si_2$ samples [20].

In contrast to the low Ge concentrations $x = 0$ and 0.05, the higher concentration of $x = 0.13$ suppresses the valence transition. There is no significant temperature dependence in this case, as illustrated in Fig. 3(a). The sharp peak near the Fermi level associated with the Eu^{2+} $4f$ states is the highest of all measured compounds.

The results of hard x-ray momentum microscopy yield a data array of the photoemission intensity $I(E_B, k_x, k_y)$ that is simultaneously measured as a function of binding energy E_B and parallel momentum k_x, k_y. The photoemission intensity resulting from phonon scattering is considerable and superimposes the intensity from direct photoemission processes. This component can be approximated by the matrix-element-weighted density of states, which is independent of the parallel momentum [27] and depicted as the valence band energy distribution curves integrated over a planar section of the full Brillouin zone (see Fig. 3).

Figures 4(a)–4(h) illustrate the alteration in the constant energy intensity maps, $I(E_B, k_x, k_y)$, between temperatures of 33 K and 140 K for the specific case of $x = 0.05$. At 33 K, the section at the Fermi level [Fig. 4(d)] in the Γ-Σ-X plane exhibits ellipses centered on the X-points, which are the brightest features, with the long axis oriented along the Γ-X direction. At room temperature, the high photoemission intensity at the X-points is no longer visible [Fig. 4(h)]. Instead, a high intensity now occurs at the Γ-points. The opposite intensity behavior occurs at $E_B = 1$ eV. Here, a high intensity occurs at the Γ-points at 33 K, while the intensity has vanished at 140 K.

In order to emphasize the band dispersion, we divided the momentum-resolved intensity, $I(E_B, k_x, k_y)$, by the integrated intensity within the Brillouin zone, as shown in Fig. 3(b), and subtracted the momentum-independent background intensity. It should be noted that due to this normalization the high intensity of the flat (dispersion-less) Eu $4f$ and Pd $4d$ bands at $E_B = 0.5$ and 3.5 eV do not appear in this representation.

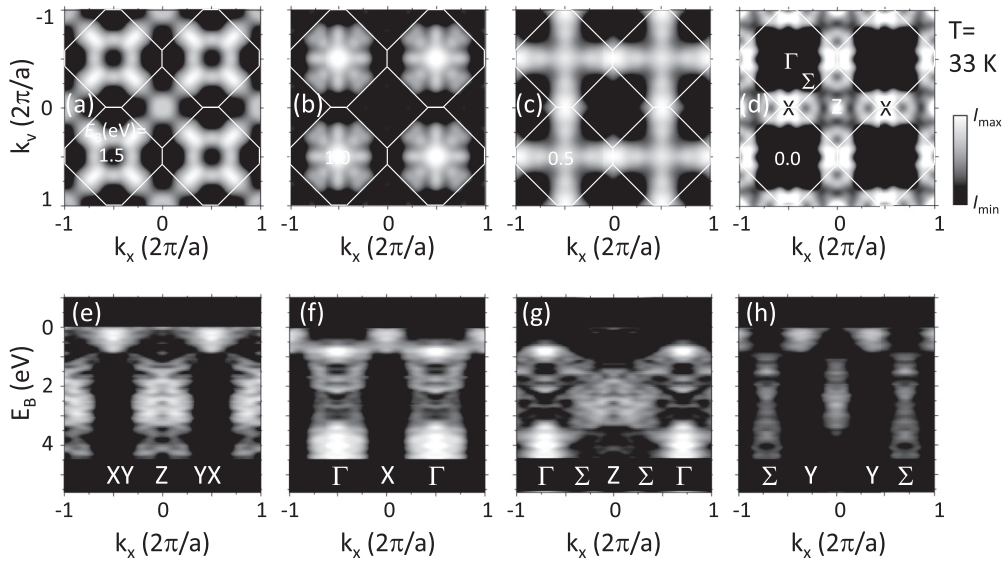

FIG. 5. (a)–(h) $EuPd_2(Si_{1-x}Ge_x)_2$ with $x = 0.13$. Constant energy maps of the photoemission intensity $I(E_B, k_x, k_y)$ for the indicated binding energies E_B measured at 33 K (a)–(d). The photon energy is 4.9 keV. The photoemission intensity has been symmetrized according to the crystal symmetry. (i)–(p) Binding energy versus parallel momentum sections of the photoemission data array along the indicated high symmetry directions measured at 33 K (e)–(h). The photoemission intensity is normalized on the valence band energy distribution curve shown in Fig. 3(a) and color coded on the indicated linear black-white scale.

Following this data processing, the band dispersion of the conduction bands is clearly visible [see Figs. 4(i)–4(p)]. It should be noted, however, that the energy resolution is insufficient to observe any hybridization of the localized Eu $4f$ with other valence states, which has been observed with higher energy resolution [36].

At 33 K, the corresponding intensity distribution demonstrates the presence of electron bands in proximity to the X-points, exhibiting electron-like, parabolic dispersion characteristics and a maximum binding energy of 0.5 eV [for details, please refer to Figs. 4(i), 4(j), and 4(l)]. The effective mass of this band is equal to the mass of the electron in the vacuum, $m/m_0 = 1$. At 140 K, the band has shifted to above the Fermi level and is no longer discernible [see Figs. 4(m), 4(o), and 4(p)]. Given that this change is accompanied by a valence change from trivalent Eu^{3+} to divalent Eu^{2+}, it seems plausible to suggest that the electron occupying the free-electron-like state at low temperature has become localized at 140 K. This would explain the increase in the peak at $E_B = 0.5$ eV, as illustrated in Fig. 3(b).

A pronounced band dispersion is observed along the Y-Σ direction [Fig. 4(l)], with a mean binding energy of $E_B =$ 1 eV and an energy width of 1 eV. The maxima are located at the Σ-points, while the minima are situated at the Y-points. At 140 K, this band has shifted to higher binding energies and has become partly unoccupied near the Σ-points.

These results are, to some extent, similar to those previously published for $x = 0$ [28]. The replacement of 5% of the Si atoms by Ge atoms results in a significant shift in transition temperature, while the dispersion behavior and its behavior above and below the transition temperature remain largely unchanged. In this sense, the substitution can be considered to act as a negative pressure, which is in accordance with expectations.

We now consider the case of $x = 0.13$, which is located in close proximity to the critical end point. As previously demonstrated by the XPS data, the valence transition does not occur between 27 K and room temperature [Fig. 1(a)]. Furthermore, the integrated valence band intensity shows no notable variation within this temperature range. Figure 5 illustrates the corresponding momentum dependence of the valence band states at 33 K. The data has been processed in a manner analogous to that employed for the data presented in Fig. 4. Note that in this case the photon energy is 4.9 keV. The higher photon energy in general leads to a decreased cross-section for photoemission, whereby the decrease is larger for larger orbital angular momentum. States with the same orbital angular momentum decrease with the same factor [32]. The apparent lack of intensity below 1.5 eV around the X and Y points in Figs. 5(e), 5(f), and 5(h) is due to the color scale focusing on details at the Fermi level.

As illustrated in Fig. 5(d), the constant-energy section of the Fermi surface for the function $I(E_B, k_x, k_y)$ reveals the presence of rectangular-shaped regions of high intensity centered at the X-points. The intensity minima are observed at the Γ-points. At a binding energy of $E_B = 1$ eV, high intensity is observed at the Γ-points, while the intensity is lower at the X-points. This is noteworthy as these bands bear resemblance to the result for $x = 0.05$ discussed previously and $x = 0$ [28], despite the valence state being that of the high temperature phase of pristine $EuPd_2Si_2$.

In contrast to $EuPd_2(Si_{1-x}Ge_x)_2$ with $x = 0$ and $x = 0.05$, the constant energy section at $E_B = 0.5$ eV demonstrates a notable absence of dispersion along the Γ-X directions [Fig. 5(c)], forming narrow lines of high intensity. The flat bands are thus constrained along the Γ-X high-symmetry directions, which may be related to the anticipated onset of strong fluctuations in the vicinity of the critical end point.

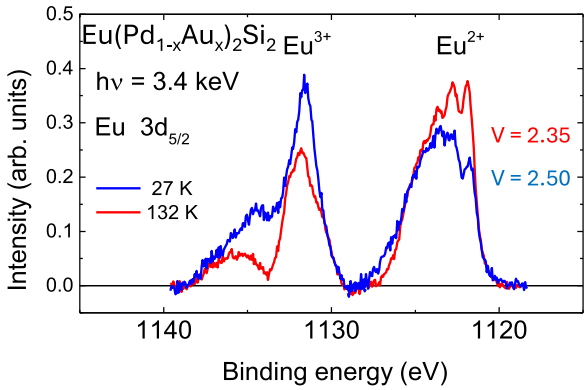

FIG. 6. (a) Temperature dependence of the Eu $3d_{5/2}$ core level spectra obtained with a photon energy of 3.4 keV at the indicated temperatures for a $Eu(Pd_{1-x}Au_x)_2Si_2$ single crystals with $x = 0.03$. The Eu valence v is calculated from the ratio of the areas of the corresponding $3d$ core level peaks. The specified binding energies are referred to the Fermi level.

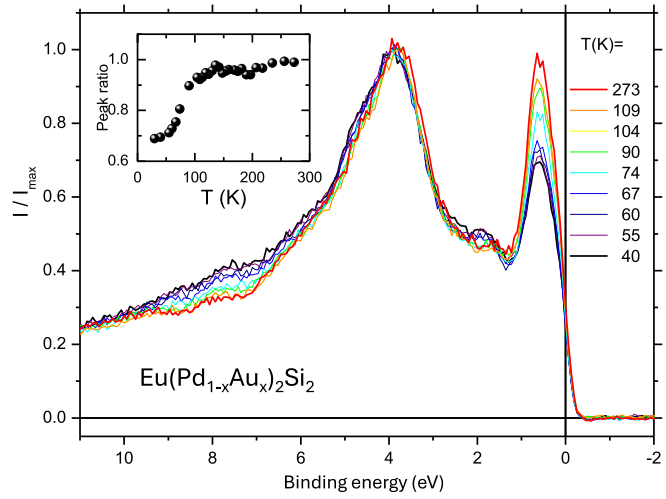

FIG. 7. Valence band energy distribution curves for the indicated temperatures for $Eu(Pd_{1-x}Au_x)_2Si_2$ with $x = 0.03$. The photoemission intensity was integrated over a planar section of the full Brillouin zone. The inset shows the temperature dependence of the peak ratio.

A second noteworthy observation is the apparent splitting of the electron-like bands in the vicinity of the X-points, with the apex at $E_B = 0.2$ and 0.5 eV. This splitting may be attributed to the onset of antiferromagnetism, which is evidenced by the corresponding exchange splitting of 0.3 eV.

IV. EXPERIMENTAL RESULTS FOR $Eu(Pd_{1-x}Au_x)_2Si_2$

The partial substitution of Pd by the larger Au atoms causes a negative pressure, too. In fact, the $Eu(Pd_{1-x}Au_x)_2Si_2$ system was the first system to study the influence of doping on the valence transition [3]. A possible coexistence of both mixed valence and magnetic order has been detected. Below a critical concentration of $x = 0.175$ the system behaved mixed valent, above this concentration (up to $x = 0.25$) the system ordered magnetically keeping a weak mixed valent character [3]. The $Eu(Pd_{1-x}Au_x)_2Si_2$ system showed an increasing instability of the magnetic Eu^{2+} ground state configuration from $x = 1$ to 0.18 [37].

Here, a comparison of the high (132 K) and low (27 K) temperature spectra of $Eu(Pd_{1-x}Au_x)_2Si_2$ with $x = 0.03$ shows a significant change in the ratio between the Eu^{2+} and Eu^{3+} components (Fig. 6). An evaluation of the peak area ratio results in values for the valence number $V = 2.35$ for $T > T_V$, corresponding to a prevailing Eu^{2+} ionization state, and an increase to $V = 2.5$ at low temperature, indicating a mixed Eu^{2+}/Eu^{3+} valence state.

To study the influence of the valence transition region on the valence band in more detail, we measured the temperature dependence of the integrated valence band intensity. Figure 7 shows the result, indicating a significant decrease of the Eu $4f$ intensity peak at $E_B = 0.5$ eV related to the Eu^{2+} ionization state with decreasing temperature. The intensity at $E_B = 8$ eV, related to the Eu $4f$ states of Eu^{3+} increases instead. This behavior is qualitatively similar as the results for $EuPd_2(Si_{1-x}Ge_x)_2$ shown in Fig. 3. In contrast to $EuPd_2(Si_{1-x}Ge_x)_2$ the Eu $4f$ states of Eu^{3+} at $E_B = 8$ eV show the typical $4f$ multiplet of the mixed valence state in the high temperature phase, too. This indicates that the valence transition to the high temperature state is not as complete as for $EuPd_2(Si_{1-x}Ge_x)_2$.

The ratio of the intensity peak at $E_B = 0.5$ eV and 3.5 eV, shown in the inset of Fig. 7, reveals a transition temperature at 75 K in good agreement with previously published results [3].

Figure 8 shows the momentum-dependent photoemission intensities for $Eu(Pd_{1-x}Au_x)_2Si_2$ with $x = 0.03$. At 25 K, the constant energy intensity map $I(E_B, k_x, k_y)$ at the Fermi level [Fig. 8(d)] in the Γ-Σ-X plane shows high circular shaped intensities at the X-points. These high intensity areas shrink at $E_B = 0.5$ eV and at $E_B = 1$ eV circles of high intensity appear around the Γ points. At 190 K above T_V, the high photoemission intensity at the X-points becomes lower and elongated along the Γ-X direction [Fig. 8(h)]. Instead a high intensity now occurs at the Γ points. At $E_B = 1$ eV [Fig. 8(f)] the circles of high intensity are much larger and the areas of high intensity are shifted to the Σ-points.

At low temperature, the band dispersion patterns show the electron bands near the X-points with an electron-like parabolic dispersion and a maximum binding energy of 0.2 eV [see Figs. 8(i), 8(j), and 8(l)]. At 190 K, this band has shifted to the Fermi level and is just barely visible [see Figs. 8(m), 8(o), and 8(p)]. Therefore, the behavior of these electron-like bands is similar to the case of $EuPd_2(Si_{1-x}Ge_x)_2$ with $x = 0.05$.

In contrast to the case of $EuPd_2(Si_{1-x}Ge_x)_2$, a second electron-like band crosses the Fermi level at the Γ-point both at low and high temperature. In addition, the band with mean value at $E_B = 1$ eV appearing in the Γ-X direction [see Fig. 8(j)] has a width of 1.5 eV, whereas it is 1 eV in the case of $EuPd_2(Si_{1-x}Ge_x)_2$ with $x = 0.05$.

These results indicate that the substitution of Pd by Au not only acts like a negative pressure, but also changes the electronic structure in a more drastic way. This can be explained by the fact that Au is not isoelectric with Pd.

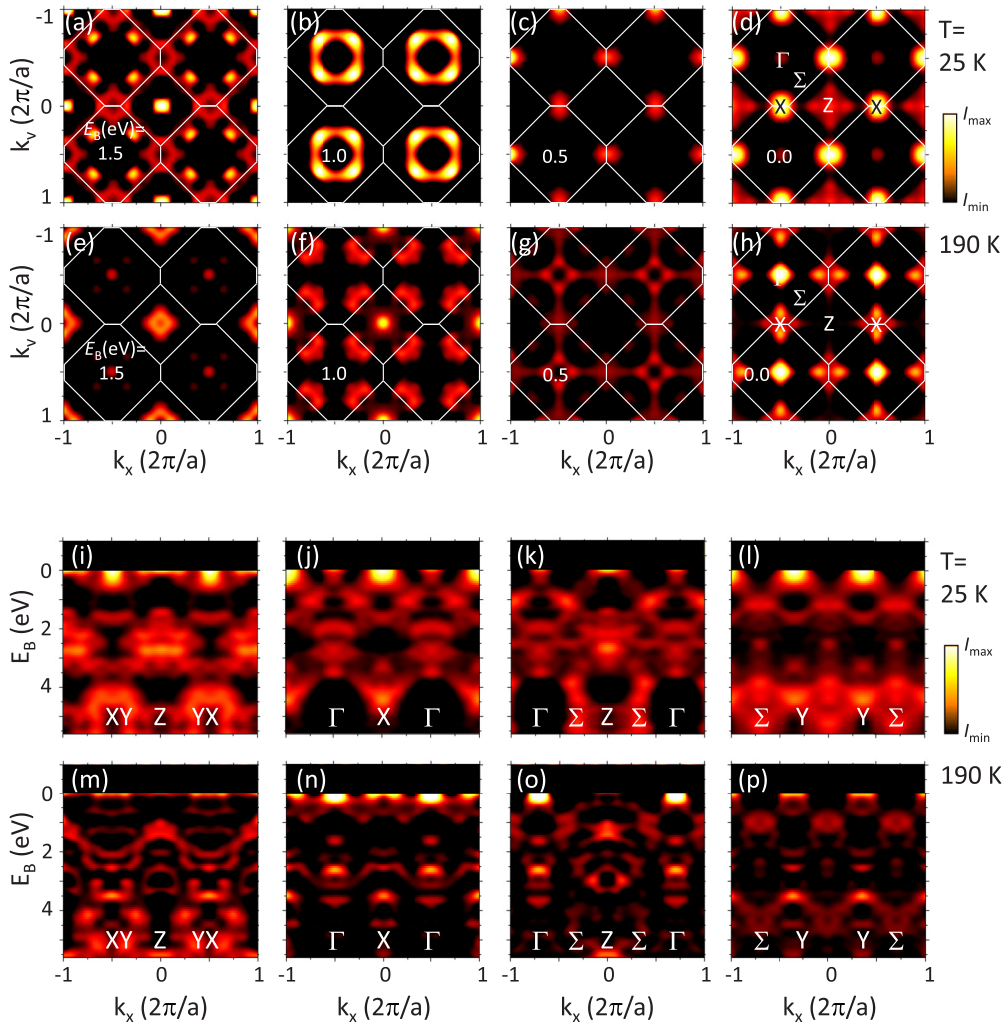

FIG. 8. (a)–(h) $Eu(Pd_{1-x}Au_x)_2Si_2$ with $x = 0.03$. Constant energy maps of the photoemission intensity $I(E_B, k_x, k_y)$ for the indicated binding energies E_B measured at 25 K (a)–(d) and 190 K (e)–(h). The photon energy is 3.4 keV. The photoemission intensity has been symmetrized according to the crystal symmetry. (i)–(p) Binding energy versus parallel momentum sections of the photoemission data array along the indicated high symmetry directions measured at 25 K (i)–(l) and 190 K (m)–(p). The photoemission intensity is normalized on the valence band energy distribution curve shown in Fig. 3(b) and color coded on the indicated linear orange-hot scale.

Instead, the Au atom adds one electron more to the valence band as compared to Pd.

V. DFT CALCULATIONS

Density functional theory (DFT)-based *ab initio* calculations were carried out for $EuPd_2(Si_{1-x}Ge_x)_2$ and $Eu(Pd_{1-x}Au_x)_2Si_2$ using the projector augmented wave method [38] implemented in the Vienna *ab initio* simulation package (VASP) [39]. To treat the exchange-correlation functional, we employed the revised generalized gradient approximation (GGA) [40,41]. The basis set size was determined by the energy cutoff of 500 eV and the first Brillouin zone was sampled by a Γ-centered $21 \times 21 \times 21$ k-mesh. Virtual crystal approximation (VCA), as implemented in VASP [42], was utilized to incorporate doping effects and to fix a desired valence state of Eu, while preserving the body-centered tetragonal symmetry. For the latter, two pseudopotentials for Eu—Eu_2 and Eu_3, representing fixed divalent or trivalent Eu, respectively, with Eu $4f$ treated as core states, were used in the calculations. These pseudopotentials were combined with a mixing factor α, defined as (1-α)(Eu_2) + α(Eu_3), where the valence number (V) of Eu is expressed as $2 + \alpha$. The same internal parameters of $EuPd_2Si_2$ [28], as used in our previous study, were employed (see also Ref. [43]), and the experimentally determined parameters were utilized for $EuPd_2Ge_2$ [5] and $EuAu_2Si_2$ [44]. For $EuPd_2Ge_2$, where only the lattice parameters were provided in Ref. [5], the atomic positions of Ge ($4e$) were fully relaxed until the net force became smaller than 1 meV/Å, resulting in $z_{rel} = 0.3718$. According to our previous reports on $EuPd_2(Si_{(1-x)}Ge_x)_2$ [18], the lattice constants a and c vary by only 0.45% and 0.27%, respectively, between $x = 0$ and $x = 0.15$. While magnetism may be influenced by such subtle changes, these variations are too small to cause significant differences in the electronic structure within the framework of DFT [43]. Therefore, in this study, we have chosen to neglect these minor mechanical effects and instead focus on analyzing

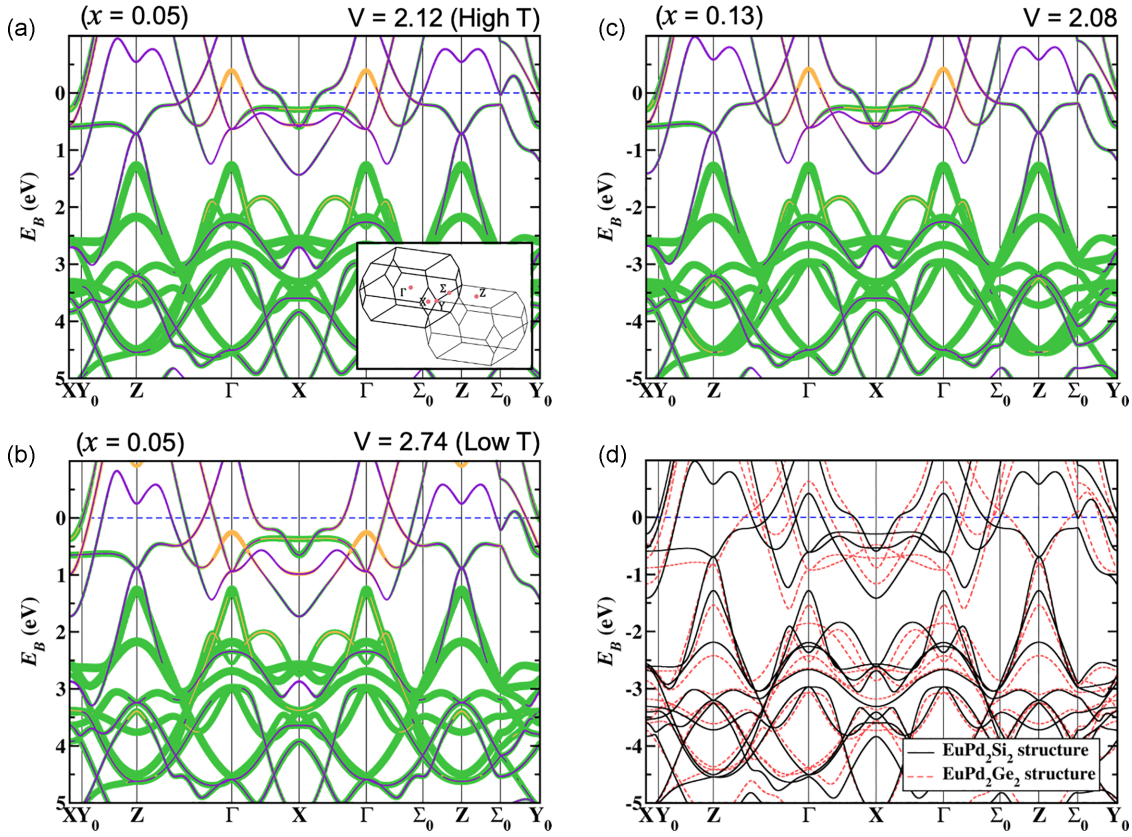

FIG. 9. Orbital-resolved band structure of $EuPd_2(Si_{1-x}Ge_x)_2$. For $x = 0.05$, the two measured V values of (a) 2.12 at high temperature and (b) 2.74 at low temperature are taken into account in calculations, whereas (c) $V = 2.08$ is used for the case of $x = 0.13$. Eu $5d$, Pd $4d$, and Si $3p$ orbitals are weighted by orange, green, and violet, respectively. (d) Overlapped band structures of $EuPd_2(Si_{1-x}Ge_x)_2$ with $V = 2.08$ and $x = 0.13$ using the internal parameters of $EuPd_2Si_2$ (black solid line) and $EuPd_2Ge_2$ (red dashed line). The inset in (a) depicts the first Brillouin zone with high-symmetry points.

how the electronic structure evolves with varying valence numbers of Eu.

We start by analyzing the $EuPd_2(Si_{1-x}Ge_x)_2$ results. Figures 9(a) and 9(b) show orbital-resolved band structures of $EuPd_2(Si_{1-x}Ge_x)_2$ with the two measured valency values $V = 2.12$ (high T) and 2.74 (low T) at $x = 0.05$ where Eu $5d$, Pd $4d$, and Si $3p$ orbitals are colored orange, green, and violet, respectively. At $V = 2.74$ (low T), an electron-like parabolic band is observed at the X point below the Fermi energy, exhibiting dominant Pd $4d$ character with a smaller contribution from Si $3p$. The minimum of this band sits at E_B of 0.78 eV and a nearly flat band intersects this parabolic band at $E_B = 0.49$ eV. Above the intersecting point, an inflection point emerges along the X to Γ path making the corresponding Fermi surface elongated along this line, which is in good agreement with the experimental observations where ellipses are found around the X points, as shown in Fig. 4(d). However, as V decreases to 2.12 (high T), this parabolic band becomes narrower shifting the inflection point above the Fermi energy. In addition, a fully occupied hole-like band at the Γ point, originating from mostly Eu $5d$, shifts above the Fermi energy, forming a hole pocket. These changes are clearly shown in the measurements, where the ellipses around the X points nearly disappear, and high intensity emerges at the Γ point as the temperature increases (see Fig. 4). When the doping level is increased to $x = 0.13$ in $EuPd_2(Si_{1-x}Ge_x)_2$, unlike the $x = 0.05$ case, the measured valence number remains nearly constant despite variations in temperature. According to our DFT calculations with $V = 2.08$ and $x = 0.13$, the band structure, shown in Fig. 9(c), is nearly similar to the one obtained using $V = 2.12$ and $x = 0.05$. However, the resulting photoemission spectra show slight differences between the two cases, as shown in Figs. 4(i)–4(l) and 5(e)–5(h).

The discrepancy between the experimental observations and the DFT calculations may arise from the fact that in the DFT calculations, the internal parameters were fixed using those of $EuPd_2Si_2$. However, replacing Si with Ge is expected to increase the system's volume [18]. This difference in volume leads to a significant variation in the electronic structure, as illustrated in Fig. 9(d), where the band structures of $EuPd_2(Si_{1-x}Ge_x)_2$ with $V = 2.08$ and $x = 0.13$ using the internal parameters of $EuPd_2Si_2$ (black solid line) and $EuPd_2Ge_2$ (red dashed line) are overlapped. Therefore, certain internal parameters interpolated between the two cases should be incorporated into the DFT calculations to achieve better agreement with the measured photoemission spectra. Additionally, it should be noted that magnetism might exist at $T = 13$ K in $EuPd_2(Si_{1-x}Ge_x)_2$ with $x = 0.13$. According to our previous study [18], antiferromagnetic long-range order was observed in $EuPd_2(Si_{1-x}Ge_x)_2$ at $x = 0.105$ with $T_N = 47$ K. T_N decreases slightly to 42 K when x is increased by 0.154. This suggests that the presence of

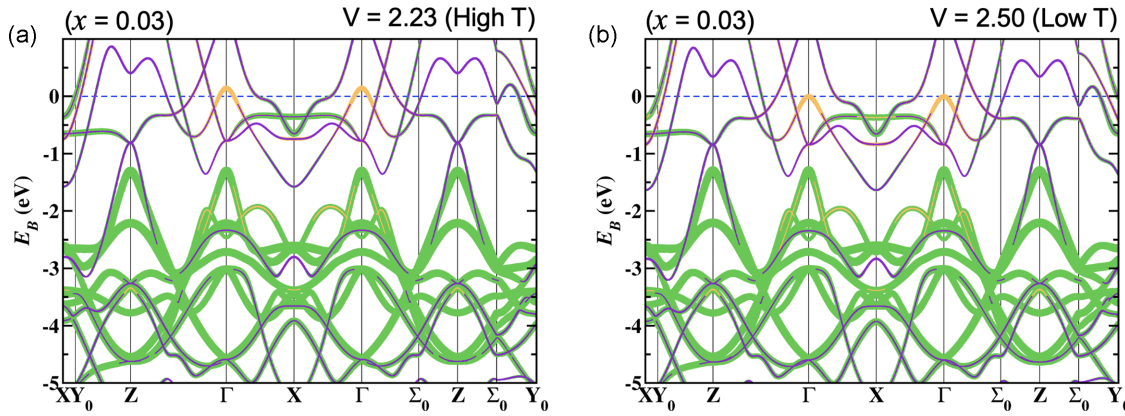

FIG. 10. Orbital resolved band structure of $Eu(Pd_{1-x}Au_x)_2Si_2$ at $x = 0.03$ using the same manner as in Fig. 9. The two measured V values of (a) 2.23 at high temperature and (b) 2.50 at low temperature are employed in the calculations.

magnetism in $EuPd_2(Si_{1-x}Ge_x)_2$ with $x = 0.13$ is highly plausible and may account for the measured photoemission spectra [Figs. 5(e)–5(h)], where nearly flat dispersions are observed. In our DFT calculations, which assume A-type antiferromagnetic ordering in $EuPd_2Ge_2$ (not shown here), similar flat bands appear due to zone folding. Consequently, our DFT approaches for doped systems with fixed V values struggle to reproduce the measured photoemission spectra, as shown in Figs. 5(e)–5(h). As mentioned above, the overall electronic structure in the presence of Ge doping is nearly similar to that of pristine $EuPd_2Si_2$, owing to the isovalency of Si and Ge. However, the effects of negative pressure and the possible emergence of magnetic long-range order induced by Ge doping introduce a substantial difference in the electronic structure.

In contrast to Ge substitution, Au doping increases the number of electrons in the system. Figure 10 illustrates the orbital-resolved band structure of $Eu(Pd_{1-x}Au_x)_2Si_2$ at $x = 0.03$ for both measured V values. Due to the small doping level, the overall electronic structure remains nearly unchanged compared to pristine $EuPd_2Si_2$. However, a noticeable difference appears in a hole-like parabolic band at the Γ point mostly originating from Eu $5d$. This band, located just above the Fermi level at $V = 2.23$, is more occupied than the corresponding band in pristine $EuPd_2Si_2$. Interestingly, the photoemission spectra reveal the emergence of an electron-like band at the Γ point at 190 K, a feature absent in the DFT results. A plausible explanation for this discrepancy could be the presence of local zone folding near the doped Au atoms. According to our DFT calculations for pure $EuAu_2Si_2$, a parabolic band at the Z point forms an electron pocket with a dominant Eu $5d$ orbital character. Considering the fact that the Z point in the $I4/mmm$ space group is folded into the Γ point in the $P4/mmm$ structure, this parabolic band could appear at the Γ point in the photoemission spectra, as shown in Fig. 8(n). However, this explanation needs to be further investigated in future studies.

VI. DISCUSSION

Figure 11(a) shows the typical temperature versus pressure phase diagram for the valence transition compounds [5]. In this context T_V represents the temperature at which the first-order valence transition temperature occurs between the high-temperature divalent Eu state and the low-temperature mixed-valent Eu^{2+}/Eu^{3+} phase. In the case of the $EuPd_2Si_2$ system, previously published data have been compiled from Refs. [3,6,18]. The valence transition temperature decreases with increasing substitution x in $EuPd_2(Si_{1-x}Ge_x)_2$ and $Eu(Pd_{1-x}Au_x)_2Si_2$, with substitution of atoms by larger ones acting in a manner analogous to that of negative pressure. The

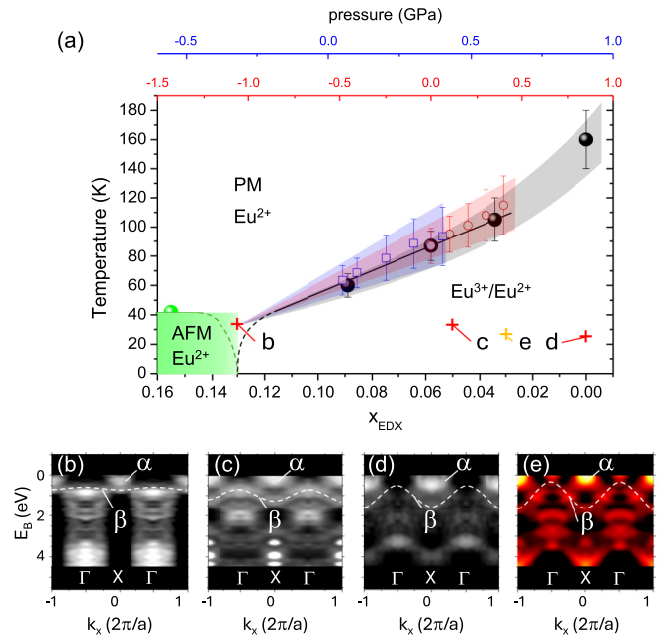

FIG. 11. (a) Phase diagram of the $EuPd_2(Si_{1-x}Ge_x)_2$ system in the vicinity of the critical endpoint. Experimental data at zero pressure from Ref. [18] (black dots) are plotted as a function of x. For the pressure-dependent data from Ref. [6] for $x = 0.05$ (red circles) and $x = 0.1$ (blue squares) the pressure scales were adapted such that T_V matches the concentration-dependent data. The plus-signs mark the parameters of the band structure results shown in (b)–(e). (b) Band dispersion along the Γ-X high symmetry direction for $x = 0.13$ at $T < T_V$. (c),(d) Similar data for $x = 0.05$ and $x = 0$, respectively. The data for $x = 0$ are taken from Ref. [28]. (e) Band dispersion along the Γ-X high symmetry direction for $Eu(Pd_{1-x}Au_x)_2Si_2$ with $x = 0.03$.

substitution of large amounts of Ge or Au drives the system into a low-temperature antiferromagnetic state with a Néel temperature of 30 K. In this case, the valence transition is suppressed, and the system remains in the magnetic divalent state even at very low temperatures [3].

In order to include the pressure-dependent results for $T_V(p)$, as reported in Ref. [6], in the phase diagram shown in Fig. 11(a), the pressure scales for the compounds $EuPd_2(Si_{1-x}Ge_x)_2$ with $x = 0.05$ and $x = 0.1$ were adapted such that the corresponding zero pressure values align with the generic $T_V(x)$ transition line. Moreover, the pressure scales have been modified in a way that ensures the transition width of $T_V(p)$ aligns with that of $T_V(x)$. As pressure is reduced and the substitution concentration is increased, the transition width of both $T_V(p)$ and $T_V(x)$ decreases, as reported in Ref. [6]. The extrapolation to negative pressure or larger concentration, respectively, yields a critical concentration of $x_V = 0.13$.

The concentration, x_V, or the pressure, p_V, is indicative of the parameter at which the first-order valence transition becomes apparent. In accordance with the findings presented in Ref. [5], there is a possibility that the antiferromagnetic state may undergo a discontinuous transition with a sharp valence crossover and the emergence of quantum critical behavior in its vicinity [45,46]. This was considered to be realized in $EuCu_2Ge_2$ under pressure [47,48].

To investigate the effect of negative pressure on the electronic valence band structure in $EuPd_2Si_2$, the low-temperature photoemission data along the high-symmetry Γ-X direction is compared in Figs. 11(b)–11(e). The increasing substitution of Si by the isoelectric Ge results in a shift of the electron-like α-band centered at the X-point to lower binding energy. In the case of the critical concentration $x = 0.13$ the band is split into two subbands, indicating the onset of exchange splitting. The β-band, centered at a binding energy of 1 eV, shows a decrease in width of the dispersion with increasing Ge concentration. This reduction in width can be attributed to a decrease in hybridization with increasing atomic distances and a corresponding localization of the electronic states. At the critical concentration, the band becomes almost flat and reduced in dimensions, which can be attributed to the onset of strong fluctuations near the critical end point.

In contrast, the substitution of Pd by Au leads to the appearance of an additional electron-like band occurring at the Fermi level at the Γ-point, which is not observed in $EuPd_2(Si_{1-x}Ge_x)_2$. In addition, the β-band has a greater width than that observed in $EuPd_2(Si_{1-x}Ge_x)_2$. These discrepancies are probably due to the Au valence states, which contribute an additional electron per atom to the valence band.

VII. SUMMARY

Hard x-ray angle-resolved photoemission spectroscopy is employed to measure the bulk electronic properties of the valence transition system $EuPd_2Si_2$ with atomic Au and Ge substitutions on the Pd and Si sites, respectively. Remarkable changes in the valence band states are observed at the valence transition, where the Eu ions undergo a temperature-induced valence crossover from a magnetic Eu^{2+} state to a valence-fluctuating state at low temperatures [49]. A systematic change in the band structure is observed for the isoelectric substitution of Si by Ge in $EuPd_2(Si_{1-x}Ge_x)_2$. Our DFT results for these doping cases suggest that changes in the electronic structure are associated with both the increase in volume and the possible presence of magnetism.

In contrast, the substitution of Pd by Au in $Eu(Pd_{1-x}Au_x)_2Si_2$ results in the emergence of additional band states near the Fermi level. Previously published pressure dependent data for $EuPd_2(Si_{1-x}Ge_x)_2$ indicate that the Ge concentration of $x = 0.13$ is close to the critical end point. In this case, a splitting of the conduction band states and the appearance of flat bands with a restriction along the Γ-X directions were observed.

ACKNOWLEDGMENTS

H.J.E. thanks Denis V. Vyalikh for fruitful discussions. This work was funded by the Deutsche Forschungsgemeinschaft (DFG, German Research Foundation), Grant No. TRR288–422213477 (Projects No. B04, No. A03, and No. A05), and by the BMBF (Projects No. 05K22UM1 and No. 05K22UM4). The funding of the instrument by the Federal Ministry of Education and Research (BMBF) under the framework program ErUM is gratefully acknowledged. We thank DESY (Hamburg, Germany), a member of the Helmholtz Association HGF, for the provision of experimental facilities. Parts of this research were performed at PETRA III using beamline P22. O.F. acknowledges funding by TopDyn.

DATA AVAILABILITY

The data that support the findings of this article are not publicly available upon publication because it is not technically feasible and/or the cost of preparing, depositing, and hosting the data would be prohibitive within the terms of this research project. The data are available from the authors upon reasonable request.

[1] E. Gati, M. Garst, R. S. Manna, U. Tutsch, B. Wolf, L. Bartosch, H. Schubert, T. Sasaki, J. A. Schlueter, and M. Lang, Breakdown of Hooke's law of elasticity at the Mott critical endpoint in an organic conductor, Sci. Adv. **2**, e1601646 (2016).

[2] J. M. Lawrence, P. S. Riseborough, and R. D. Parks, Valence fluctuation phenomena, Rep. Prog. Phys. **44**, 1 (1981).

[3] C. U. Segre, M. Croft, J. A. Hodges, V. Murgai, L. C. Gupta, and R. D. Parks, Valence instability in $Eu(Pd_{1-x}Au_x)_2Si_2$: The global phase diagram, Phys. Rev. Lett. **49**, 1947 (1982).

[4] Y. Ōnuki, A. Nakamura, F. Honda, D. Aoki, T. Tekeuchi, M. Nakashima, Y. Amako, H. Harima, K. Matsubayashi, Y. Uwatoko, S. Kayama, T. Kagayama, K. Shimizu, S. E. Muthu, D. Braithwaite, B. Salce, H. Shiba, T. Yara, Y. Ashitomi, H.

Akamine *et al.*, Divalent, trivalent, and heavy fermion states in Eu compounds, Philos. Mag. **97**, 3399 (2016).

[5] Y. Ōnuki, M. Hedo, and F. Honda, Unique electronic states of Eu-based compounds, J. Phys. Soc. Jpn. **89**, 102001 (2020).

[6] B. Wolf, F. Spathelf, J. Zimmermann, T. Lundbeck, M. Peters, K. Kliemt, C. Krellner, and M. Lang, From magnetic order to valence-change crossover in $EuPd_2(Si_{1-x}Ge_x)_2$ using He-gas pressure, SciPost Phys. Proc. **11**, 022 (2023).

[7] E. R. Bauminger, D. Froindlich, I. Nowik, S. Ofer, I. Felner, and I. Mayer, Charge fluctuations in europium in metallic $EuCu_2Si_2$, Phys. Rev. Lett. **30**, 1053 (1973).

[8] S. Patil, R. Nagarajan, C. Godart, J. P. Kappler, L. C. Gupta, B. D. Padalia, and R. Vijayaraghavan, Valence fluctuation in the dilute Eu systems Eu: RPd_2Si_2, Eu: RCu_2Si_2, and Eu: RNi_2Si_2 (R = La, Y, and Yb), Phys. Rev. B **47**, 8794 (1993).

[9] S. Schulz, I. A. Nechaev, M. Güttler, G. Poelchen, A. Generalov, S. Danzenbächer, A. Chikina, S. Seiro, K. Kliemt, A. Y. Vyazovskaya, T. K. Kim, P. Dudin, E. V. Chulkov, C. Laubschat, E. E. Krasovskii, C. Geibel, C. Krellner, K. Kummer, and D. V. Vyalikh, Emerging 2D-ferromagnetism and strong spin-orbit coupling at the surface of valence-fluctuating $EuIr_2Si_2$, npj Quantum Mater. **4**, 26 (2019).

[10] B. Chevalier, J. M. D. Coey, B. Lloret, and J. Etourneau, $EuIr_2Si_2$: A new intermediate valence compound, J. Phys. C **19**, 4521 (1986).

[11] S. Seiro, Y. Prots, K. Kummer, H. Rosner, R. C. Gil, and C. Geibel, Charge, lattice and magnetism across the valence crossover in $EuIr_2Si_2$, J. Phys.: Condens. Matter **31**, 305602 (2019).

[12] A. Mitsuda, S. Hamano, N. Araoka, H. Yayama, and H. Wada, Pressure-induced valence transition in antiferromagnet $EuRh_2Si_2$, J. Phys. Soc. Jpn. **81**, 023709 (2012).

[13] A. Nakamura, T. Nakama, K. Uchima, N. Arakaki, C. Zukeran, S. Komesu, M. Takeda, Y. Takaesu, D. Nakamura, M. Hedo, K. Yagasaki, and Y. Uwatoko, Effect of pressure on thermopower of $EuNi_2Ge_2$, J. Phys.: Conf. Ser. **400**, 032106 (2012).

[14] G. Dionicio, H. Wilhelm, Z. Hossain, and C. Geibel, Temperature- and pressure-induced valence transition in C_6Yb and C_6Ca, Phys. B: Condens. Matter **378–380**, 724 (2006).

[15] K. Ichiki, K. Mimura, H. Anzai, T. Uozumi, H. Sato, Y. Utsumi, S. Ueda, A. Mitsuda, H. Wada, Y. Taguchi, K. Shimada, H. Namatame, and M. Taniguchi, Hard x-ray photoemission study of the temperature-induced valence transition system $EuNi_2Si_2$, Phys. Rev. B **96**, 045106 (2017).

[16] Y. Yokoyama, K. Kawakami, Y. Hirata, K. Takubo, K. Yamamoto, K. Abe, A. Mitsuda, H. Wada, T. Uozumi, S. Yamamoto, I. Matsuda, S. Kimura, K. Mimura, and H. Wadati, Photoinduced valence dynamics in $EuNi_2Si_2$ studied via time-resolved x-ray absorption spectroscopy, Phys. Rev. B **100**, 115123 (2019).

[17] K. Kliemt, M. Peters, I. Reiser, M. Ocker, F. Walther, D.-M. Tran, E. Cho, M. Merz, A. A. Haghighirad, D. C. Hezel, F. Ritter, and C. Krellner, Influence of the Pd–Si ratio on the valence transition in $EuPd_2Si_2$ single crystals, Cryst. Growth Des. **22**, 5399 (2022).

[18] M. Peters, K. Kliemt, M. Ocker, B. Wolf, P. Puphal, M. Le Tacon, M. Merz, M. Lang, and C. Krellner, From valence fluctuations to long-range magnetic order in $EuPd_2Si_2$ single crystals, Phys. Rev. Mater. **7**, 064405 (2023).

[19] N. Mårtensson, B. Reihl, W. D. Schneider, V. Murgai, L. C. Gupta, and R. D. Parks, Highly resolved surface shifts in a mixed-valent system: $EuPd_2Si_2$, Phys. Rev. B **25**, 1446 (1982).

[20] K. Mimura, Y. Taguchi, S. Fukuda, A. Mitsuda, J. Sakurai, K. Ichikawa, and O. Aita, Temperature dependence of Eu 4f states in $EuPd_2Si_2$: Bulk-sensitive high-resolution photoemission study, Phys. B: Condens. Matter **351**, 292 (2004).

[21] K. Mimura, Y. Taguchi, S. Fukuda, A. Mitsuda, J. Sakurai, K. Ichikawa, and O. Aita, Bulk-sensitive high-resolution photoemission study of a temperature-induced valence transition system $EuPd_2Si_2$, J. Electron Spectrosc. Relat. Phenom. **137–140**, 529 (2004).

[22] E. V. Sampathkumaran, L. C. Gupta, R. Vijayaraghavan, K. V. Gopalakrishnan, R. G. Pillay, and H. G. Devare, A new and unique Eu-based mixed valence system: $EuPd_2Si_2$, J. Phys. C **14**, L237 (1981).

[23] M. Croft, J. A. Hodges, E. Kemly, A. Krishnan, V. Murgai, and L. C. Gupta, Cooperative configuration change in $EuPd_2Si_2$, Phys. Rev. Lett. **50**, 1534(E) (1983).

[24] D. M. Adams, A. E. Heath, H. Jhans, A. Norman, and S. Leonard, The effect of high pressure upon the valence transition in $EuPd_2Si_2$, J. Phys.: Condens. Matter **3**, 5465 (1991).

[25] A. Mitsuda, H. Wada, M. Shiga, H. A. Katori, and T. Goto, Field-induced valence transition of $Eu(Pd_{1-x}Pt_x)_2Si_2$, Phys. Rev. B **55**, 12474 (1997).

[26] K. K. Iyer, T. Basu, P. Paulose, and E. Sampathkumaran, Eu valence transition behavior in the nano form of $EuPd_2Si_2$, J. Magn. Magn. Mater. **465**, 515 (2018).

[27] S. Kölsch, A. Schuck, M. Huth, O. Fedchenko, D. Vasilyev, S. Chernov, O. Tkach, H.-J. Elmers, G. Schöönhense, C. Schlüter, T. R. F. Peixoto, A. Gloskowski, and C. Krellner, Clamping effect on temperature-induced valence transition in epitaxial $EuPd_2Si_2$ thin films grown on MgO(001), Phys. Rev. Mater. **6**, 115003 (2022).

[28] O. Fedchenko, Y.-J. Song, O. Tkach, Y. Lytvynenko, S. V. Chernov, A. Gloskovskii, C. Schlueter, M. Peters, K. Kliemt, C. Krellner, R. Valentí, G. Schönhense, and H. J. Elmers, Valence transition induced changes of the electronic structure in $EuPd_2Si_2$, Phys. Rev. B **109**, 085130 (2024).

[29] C. Schlueter, A. Gloskovskii, K. Ederer, I. Schostak, S. Piec, I. Sarkar, Y. Matveyev, P. Lömker, M. Sing, R. Claessen, C. Wiemann, C. M. Schneider, K. Medjanik, G. Schönhense, P. Amann, A. Nilsson, and W. Drube, The new dedicated HAXPES beamline P22 at PETRAIII, in *13th International Conference on Synchrotron Radiation Instrumentation, SRI2018, Taipei, Taiwan*, AIP Conf. Proc. No. 2054 (AIP, New York, 2019), p. 040010.

[30] K. Medjanik, S. V. Babenkov, S. Chernov, D. Vasilyev, B. Schönhense, C. Schlueter, A. Gloskovskii, Y. Matveyev, W. Drube, H. J. Elmers, and G. Schönhense, Progress in HAXPES performance combining full-field *k*-imaging with time-of-flight recording, J. Synchrotron Radiat. **26**, 1996 (2019).

[31] K. Medjanik, O. Fedchenko, S. Chernov, D. Kutnyakhov, M. Ellguth, A. Oelsner, B. Schönhense, T. R. F. Peixoto, P. Lutz, C.-H. Min, F. Reinert, S. Däster, Y. Acremann, J. Viefhaus, W. Wurth, H. J. Elmers, and G. Schönhense, Direct 3D mapping of the Fermi surface and Fermi velocity, Nat. Mater. **16**, 615 (2017).

[32] S. Babenkov, K. Medjanik, D. Vasilyev, S. Chernov, C. Schlueter, A. Gloskovskii, Y. Matveyev, W. Drube, B.

Schönhense, K. Rossnagel, H.-J. Elmers, and G. Schönhense, High-accuracy bulk electronic bandmapping with eliminated diffraction effects using hard x-ray photoelectron momentum microscopy, Commun. Phys. **2**, 107 (2019).

[33] M. P. Seah and W. A. Dench, Quantitative electron spectroscopy of surfaces: A standard data base for electron inelastic mean free paths in solids, Surf. Interface Anal. **1**, 2 (1979).

[34] K. Mimura, T. Uozumi, T. Ishizu, S. Motonami, H. Sato, Y. Utsumi, S. Ueda, A. Mitsuda, K. Shimada, Y. Taguchi, Y. Yamashita, H. Yoshikawa, H. Namatame, M. Taniguchi, and K. Kobayashi, Temperature-induced valence transition of $EuPd_2Si_2$ studied by hard x-ray photoelectron spectroscopy, Jpn. J. Appl. Phys. **50**, 05FD03 (2011).

[35] F. Gerken, Calculated photoemission spectra of the 4*f* states in the rare-earth metals, J. Phys. F **13**, 703 (1983).

[36] S. Danzenbächer, D. V. Vyalikh, Y. Kucherenko, A. Kade, C. Laubschat, N. Caroca-Canales, C. Krellner, C. Geibel, A. V. Fedorov, D. S. Dessau, R. Follath, W. Eberhardt, and S. L. Molodtsov, Hybridization phenomena in nearly-half-filled f -shell electron systems: Photoemission study of $EuNi_2P_2$, Phys. Rev. Lett. **102**, 026403 (2009).

[37] M. Abd-Elmeguid, C. Sauer, U. Köbler, W. Zinn, J. Röhler, and K. Keulerz, Valence instability in magnetically ordered $Eu(Pd_{1-x}Au_x)_2Si_2$, J. Magn. Magn. Mater. **47-48**, 417 (1985).

[38] P. E. Blöchl, Projector augmented-wave method, Phys. Rev. B **50**, 17953 (1994).

[39] G. Kresse and J. Furthmüller, Efficient iterative schemes for *ab initio* total-energy calculations using a plane-wave basis set, Phys. Rev. B **54**, 11169 (1996).

[40] J. P. Perdew, K. Burke, and M. Ernzerhof, Generalized gradient approximation made simple, Phys. Rev. Lett. **77**, 3865 (1996).

[41] J. P. Perdew, A. Ruzsinszky, G. I. Csonka, O. A. Vydrov, G. E. Scuseria, L. A. Constantin, X. Zhou, and K. Burke, Restoring the density-gradient expansion for exchange in solids and surfaces, Phys. Rev. Lett. **100**, 136406 (2008).

[42] C. Eckhardt, K. Hummer, and G. Kresse, Indirect-to-direct gap transition in strained and unstrained Sn_xGe_{1-x} alloys, Phys. Rev. B **89**, 165201 (2014).

[43] Y.-J. Song, S. Schulz, K. Kliemt, C. Krellner, and R. Valentí, Microscopic analysis of the valence transition in tetragonal $EuPd_2Si_2$, Phys. Rev. B **107**, 075149 (2023).

[44] I. Mayer, J. Cohen, and I. Felner, The crystal structure of the MAu_2Si_2 rare earth compounds, J. Less-Common Met. **30**, 181 (1973).

[45] S. Watanabe and K. Miyake, Origin of drastic change of Fermi surface and transport anomalies in $CeRhIn_5$ under pressure, J. Phys. Soc. Jpn. **79**, 033707 (2010).

[46] S. Watanabe and K. Miyake, Roles of critical valence fluctuations in Ce- and Yb-based heavy fermion metals, J. Phys.: Condens. Matter **23**, 094217 (2011).

[47] J. Gouchi, K. Miyake, W. Iha, M. Hedo, T. Nakama, Y. Ōnuki, and Y. Uwatoko, Quantum criticality of valence transition for the unique electronic state of antiferromagnetic compound $EuCu_2Ge_2$, J. Phys. Soc. Jpn. **89**, 053703 (2020).

[48] W. Iha, T. Yara, Y. Ashitomi, M. Kakihana, T. Takeuchi, F. Honda, A. Nakamura, D. Aoki, J. Gouchi, Y. Uwatoko, T. Kida, T. Tahara, M. Hagiwara, Y. Haga, M. Hedo, T. Nakama, and Y. Ōnuki, Electronic states in $EuCu_2(Ge_{1-x}Si_x)_2$ based on the Doniach phase diagram, J. Phys. Soc. Jpn. **87**, 064706 (2018).

[49] M. Croft, J. A. Hodges, E. Kemly, A. Krishnan, V. Murgai, and L. C. Gupta, Cooperative configuration change in $EuPd_2Si_2$, Phys. Rev. Lett. **48**, 826 (1982).